Received 25 June 2021
Revised 18 September 2021
Accepted 3 November 2021

Modeling anisotropic magnetic hysteresis properties with vector stop model by using finite element method

Xiao Xiao, Fabian Müller, Martin Marco Nell and Kay Hameyer
Institute of Electrical Machines (IEM), RWTH Aachen University, Aachen, Germany

Abstract

Purpose – This paper aims to use a history-dependent vector stop hysteresis model incorporated into a two dimensional finite elements (FE) simulation environment to solve the magnetic field problems in electrical machines. The vector stop hysteresis model is valid for representing the anisotropic magnetization characteristics of electrical steel sheets. Comparisons of the simulated results with measurements show that the model is well appropriate for the simulation of electrical machines with alternating, rotating and harmonic magnetic flux densities.

Design/methodology/approach – The anisotropy of the permeability of an electrical steel sheet can be represented by integrating anhysteretic surfaces into the elastic element of a vector hysteresis stop model. The parameters of the vector stop hysteresis model were identified by minimizing the errors between the simulated results and measurements. In this paper, a damped Newton method is applied to solve the nonlinear problem, which ensures a robust convergence of the finite elements simulation with vector stop hysteresis model.

Findings – Analyzing the measurements of the electrical steel sheets sample obtained from a rotational single sheet tester shows the importance to consider the anisotropic and saturation behavior of the material. Comparing the calculated and measured data corroborates the hypothesis that the presented energy-based vector stop hysteresis model is able to represent these magnetic properties appropriately. To ensure a unique way of hysteresis loops during finite elements simulation, the memory of the vector stop hysteresis model from last time step is kept unchanged during the Newton iterations.

Originality/value – The results of this work demonstrates that the presented vector hysteresis stop model allows simulation of vector hysteresis effects of electrical steel sheets in electrical machines with a limited amount of measurements. The essential properties of the electrical steel sheets, such as phase shifts, the anisotropy of magnetizations and the magnetization characteristics by alternating, rotating, harmonic magnetization types, can be accurately represented.

Keywords Soft magnetic materials, Magnetic hysteresis, Finite element analysis, Vector stop hysteresis model, Electromagnetic fields, Finite element method, Magnetic nonlinearity, Computational electromagnetics

Paper type Research paper

1. Introduction

In the conventional modeling of static magnetic hysteresis effects, the isotropic hysteresis models are constructed, which can be simplified to the scalar hysteresis

Thanks to Dr Klaus Kuhnen of Robert Bosch GmbH for sharing his experiences in hysteresis modeling. The German Research Foundation (DFG) supported this work within the research project number 373150943 "Vector hysteresis modeling of ferromagnetic materials."

COMPEL - The international journal for computation and mathematics in electrical and electronic engineering
Vol. 41 No. 2, 2022
pp. 752-763

0332-1649
DOI 10.1108/COMPEL-06-2021-0213

model by neglecting the anisotropic behavior of soft magnetic materials (Bastos and Sadowski, 2017; Dlala, *et al.*, 2006). Although an isotropic property is expected for non-oriented (NO) electrical steel sheets, a weak anisotropy effect can still be noticed (Shiozaki and Kurosaki, 1989; Chwastek, 2013). To represent the magnetic anisotropy referenced to the amplitude and direction of the applied magnetic field, different vector hysteresis models are developed and proposed. A vectorized model can be constructed by superposition of scalar hysteresis models from different directions (Mayergoyz, 1991; Matsuo and Shimasaki, 2001). An alternative is to directly construct the model with vectorized play or stop operators (Leite, *et al.*, 2007; Steentjes, *et al.*, 2016). According to the mechanical analogy and an energy point of view, the operator can be decomposed into elastic and plastic components (Bergqvist, *et al.*, 1997). Applying the rheological elements to represent these elastic and plastic elements, the constructed model is thermodynamic consistent. Therefore, the anhysteretic component is represented by a spring and the irreversible part is implemented by a dry friction element (Bergqvist, 1997).

The anisotropic permeability of the electrical steel sheets can be represented by integrating the anisotropy characteristics into the elastic elements of the vector stop hysteresis model. There are several approaches to simulate these anisotropic anhysteretic characteristics. Large amounts of models use analytical formulations such as the double Langevin function (Longhitano, *et al.*, 2019; Leite, *et al.*, 2004), the Elliot transfer function or the Exponential function (Bastos, *et al.*, 2018). Alternatively, the anhysteretic models can be constructed with the energy or co-energy density and the anisotropic anhysteretic behavior is considered by the equal contours of these energy densities (Silvester and Gupta, 1991; Pera, *et al.*, 1993). In this paper, the anhysteretic part of the model is implemented by the algebraic anisotropic anhysteretic model (Bavendiek, *et al.*, 2019), which delivers the anhysteretic surfaces with the relationships of $H(B)$. These surfaces are obtained by interpolating the approximated anhysteretic curves from alternating major loops in different magnetization directions. The alternating measurements of the electrical steel sheets are obtained by using a rotational single sheet tester (RSST). In the end, the vector stop hysteresis model with anisotropic characteristics is integrated into a finite element method (FEM) solver to study the influence from the hysteresis model on the distribution of the magnetic flux density in electrical machines. The model is validated with the measurements from TEAM Workshop Problem 32 (Bottauscio, *et al.*, 2002).

2. Measurements and anisotropic anhysteretic algebraic model

To study the relationship of the amplitude and phase shift between the magnetic field $\boldsymbol{H}$ and the magnetic flux density $\boldsymbol{B}$, a sample with a thickness of 0.5 mm and a square shape of 60 × 60 mm is characterized in the RSST. The square sample is from the NO soft magnetic material M330-35 (2.4 Wt.% Si) and is excited by magnetic flux densities from 0.1 T to 1.6 T with steps of 0.1 T. The excitation direction is along an angle from 0° to 90° in steps of 10°. To extract the approximated anhysteretic characteristics from the measurements the major loops from each excitation direction are used (Figure 1). From this figure, we can see the magnetic properties of the soft magnetic material are varied with field directions.

The approximated anhysteretic curves are the middle curves between the ascending and descending branches of each major loop. The obtained approximated anhysteretic curves are further interpolated and smoothed by cubic splines to ensure a monotonic increase of the

magnetization $\boldsymbol{B}(\boldsymbol{H})$. By using the symmetric properties of the approximated anhysteretic curves, the anhysteretic surface is modeled with the positive part of the curves (Figure 2).

Increasing the applied $\boldsymbol{H}$ field, the extrapolated magnetization curves with saturation properties are obtained by using piecewise cubic Hermite interpolating polynomial and are plotted in Figure 3. Figure 3(a) depicts that the magnetic polarization is unchanged since the material saturates. Meanwhile, the magnetic flux density is increased further with the slope of the permeability of vacuum, which is shown in Figure 3(b). The extrapolation to saturated polarization ensures the correct representation of saturation properties of the soft magnetic materials.

Furthermore, by interpolating the extrapolated magnetic curves $\boldsymbol{H}(\boldsymbol{B})$ between the excitation angles from 0° to 180°, the anhysteretic surfaces are obtained and depicted in Figure 4(a). The surfaces H_x (B_x, B_y) and H_y(B_x, B_y) depict a one-to-one relationship between the vectors $\boldsymbol{H}$ and $\boldsymbol{B}$. Vector $\boldsymbol{H}$ is monotonic increasing with $\boldsymbol{B}$ in arbitrary excitation directions. Calculating the output of the elastic component by an input induction (B_x, B_y), accordingly, H_x and H_y are obtained by interpolation from the surfaces in Figure 4(a) separately. A validation by comparison the anhysteretic characteristics calculated from

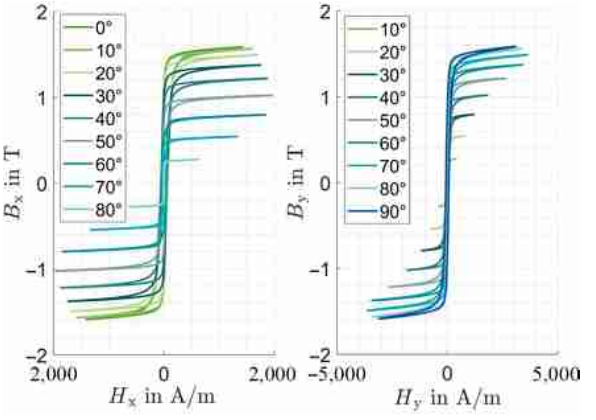

Figure 1.
Measured major loops in the magnetization direction along 0° to 90° on a magnetic amplitude of 1.6 T

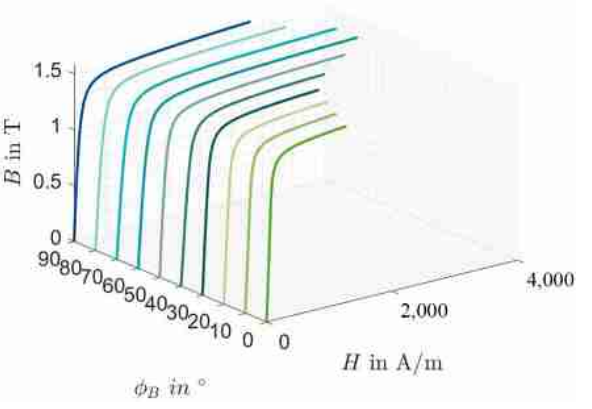

Figure 2.
Approximated anhysteretic curves derived from measured major loops in the magnetization direction along 0° to 90° of the NO soft magnetic material M330-35 (2.4 Wt.% Si)

measurements and the model is shown in Figure 4(b). It shows that the anhysteretic curves obtained from measurements is well approximated by this anisotropic anhysteretic algebraic model.

The reluctivity matrix is a 2-by-2 matrix and is derived from the partial derivative of the anhysteretic magnetization characteristics $\boldsymbol{H}(\boldsymbol{B})$, which is shown in Figure 5. Each sub-figure describes one component of the two dimensional matrix $\boldsymbol{\nu}_{\mathrm{d}}$:

$$\boldsymbol{H} = \boldsymbol{\nu}_{\mathrm{d}}\boldsymbol{B} = \begin{bmatrix} \nu_{\mathrm{xx}} & \nu_{xy} \\ \nu_{yx} & \nu_{yy} \end{bmatrix} \boldsymbol{B} = \begin{bmatrix} \dfrac{\partial H_{\mathrm{x}}}{\partial B_{\mathrm{x}}} & \dfrac{\partial H_{\mathrm{x}}}{\partial B_y} \\ \dfrac{\partial H_y}{\partial B_x} & \dfrac{\partial H_y}{\partial B_y} \end{bmatrix} \boldsymbol{B}. \tag{1}$$

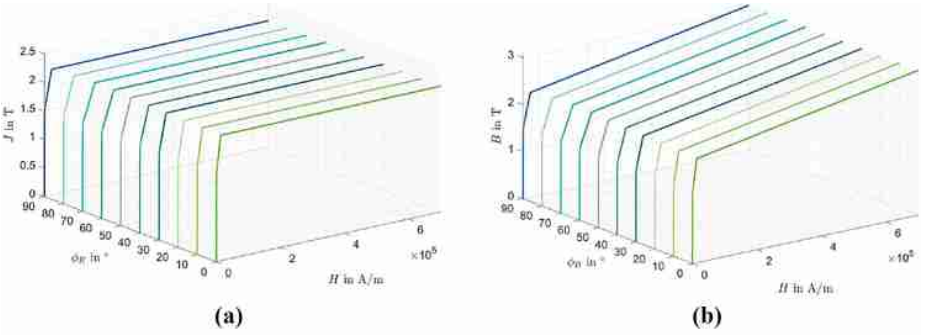

Source: (a) $J(\phi, H)$; (b) $B(\phi, H)$

Figure 3. Extrapolation of the approximated anhysteretic curves of M330-35 (2.4 Wt.% Si) to the saturation range

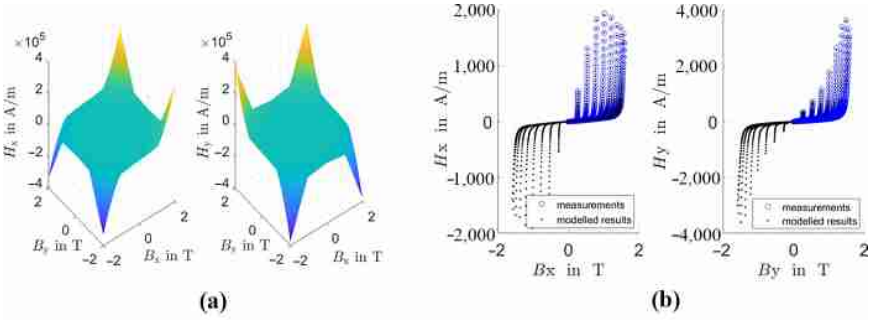

Source: (a) Hx (Bx, By) and Hy (Bx, By); (b) validation of Hx(Bx) and Hy (By)

Figure 4. Extrapolated anhysteretic surfaces of M330-35(2.4 Wt.% Si) derived from the anisotropic anhysteretic algebraic model (a); and validation of the anisotropic anhysteretic algebraic model by comparison the anhysteretic curves derived from measurements with the anhysteretic curves obtained from the model (b)

The Helmholtz free energy density f must be a convex surface to ensure the uniqueness of H, which means the differential reluctivity matrix must be positive definite (Bergqvist, 1997). The differential reluctivity is also symmetric, as it is the second derivative of the Helmholtz free energy density f:

$$\nu_{xy} = \nu_{yx} = \frac{\partial f}{\partial B_x \partial B_y} \quad . \tag{2}$$

From this anhysteretic model, the phase shifts between $\boldsymbol{B}$ and $\boldsymbol{H}$ can also be obtained in arbitrary magnetization directions. In Figure 6(a) the angles of the alternating inputs $\boldsymbol{B}$

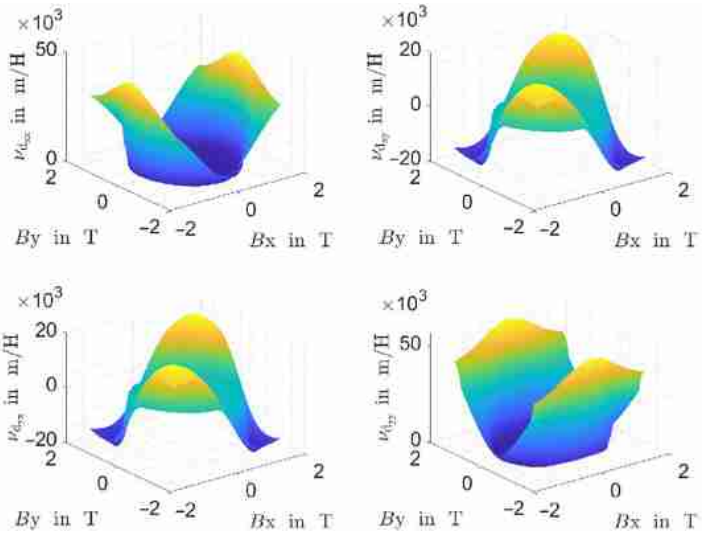

Figure 5.
Schematic representation of the differential reluctivity matrix derived from the anhysteretic surfaces of M330-35 (2.4 Wt.% Si)

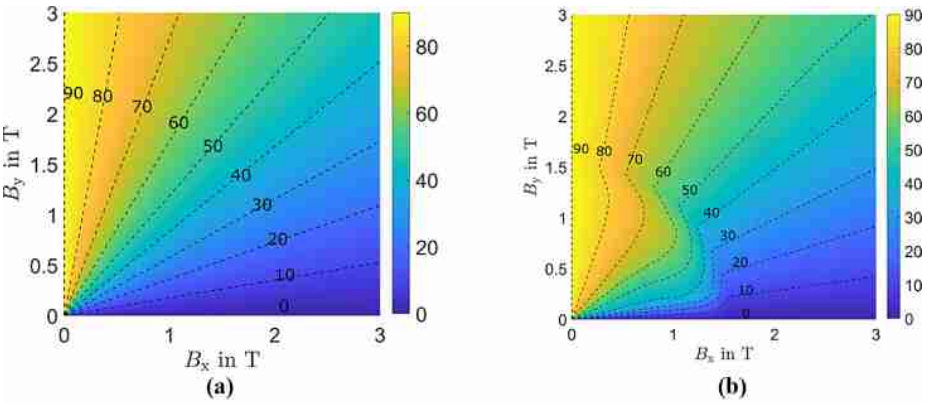

Figure 6.
Phase shifts between $\boldsymbol{B}$ and $\boldsymbol{H}$ of M330-35 (2.4 Wt.% Si)

Source: (a) φB (Bx, By); (b) φH(Bx, By)

related to the rolling direction (RD) are presented. The inputs magnetize the material in certain excitation direction from 0° to 90° in steps of 10°. The angles with respect to the RD of the corresponding output $\boldsymbol{H}$ are shown in Figure 6(b). The phase shifts between $\boldsymbol{B}$ and $\boldsymbol{H}$ are gradually vanished with higher amplitudes of magnetic flux density and the directions of the output $\boldsymbol{H}$ coincide slowly with the excitation $\boldsymbol{B}$.

The presented anisotropic anhysteretic algebraic model considers the anisotropy in magnetization, the magnetic saturation properties and the phase shifts properties. It can be used to represent the anisotropic anhysteretic properties of the elastic elements in vector stop hysteresis model.

3. Vector stop hysteresis model with anisotropic elastic element

The vector stop model can simulate the inverse relationship $\boldsymbol{H}(\boldsymbol{B})$ with vectorized stop hysterons. With a mechanical analogy, a stop operator can be represented by coupling an elastic element in series with a plastic element (Visintin, 2006). A stop hysteron $\boldsymbol{S}_n$ is defined (Leite, *et al.*, 2005) as follows:

$$\boldsymbol{S}_{\mathrm{n}} = \boldsymbol{B}_{\mathrm{re}}{}^{\mathrm{t}} = \begin{cases} \boldsymbol{\Omega}_{\mathrm{n}} & \text{if } |\boldsymbol{\eta}_{\mathrm{n}}{}^{-1}\boldsymbol{\Omega}_{\mathrm{n}}| < 1 \\ \boldsymbol{\eta}_{\mathrm{n}} \dfrac{\boldsymbol{\Omega}_{\mathrm{n}}}{|\boldsymbol{\Omega}_{\mathrm{n}}|} & \text{if } |\boldsymbol{\eta}_{\mathrm{n}}{}^{-1}\boldsymbol{\Omega}_{\mathrm{n}}| \geq 1 \end{cases}, \tag{3}$$

where $\boldsymbol{\Omega}_n = \mathrm{d}\boldsymbol{B} + \boldsymbol{S}_n{}^{t-1}$, $\mathrm{d}\boldsymbol{B} = \boldsymbol{B}^t - \boldsymbol{B}^{t-1}$ and $\boldsymbol{\eta}_n$ is the threshold diagonal matrix of the plastic dry friction element of the n-th stop operator. The parameter $\boldsymbol{\eta}$ defines the height of the stop operator and decides when the stop operator switches. The alternating loops of the stop operators rotate clockwise. The output of the stop operator $\boldsymbol{S}_n$ at the timestep t is dependent on the memory state $\boldsymbol{S}_n{}^{t-1}$ at the previous time step $t-1$. The inclusion of the memory property ensures physically correct predictions of the hysteresis branches.

In the next step, a stop model is constructed with a number of these stop operators connected in parallel and is presented as Prandtl–Ishilinskii model in (Krasnosel'skii and Pokrovskii, 1989). Each of the operators has a weight denoted with the parameter ω_{n}, which describes the contribution of each operator to the entire system. In a stop model, the strain (analog as $\boldsymbol{B}$) is the input and the stress (analog as $\boldsymbol{H}$) is the output. In a single stop operator the elastic element is collected in series with the plastic element, resulting in the same stress on the elastic spring $\boldsymbol{H}_{\mathrm{re}}$ and the friction element $\boldsymbol{H}_{\mathrm{irr}}$. Thus, only the stress on the spring has to be calculated to evaluate the output of one stop operator (Figure 7).

The anisotropic anhysteretic algebraic model $\boldsymbol{H}(\boldsymbol{S}_n)$, which represents the elastic element of the stop operator, can evaluate the stress on the spring due to its elastic deformation. The vector stop hysteresis model $\boldsymbol{H}(\boldsymbol{B})$ is computated from:

$$\boldsymbol{H}(\boldsymbol{B}) = \sum_{i=1}^{n} \omega_n f'\left(\boldsymbol{B}_{\mathrm{re}}{}^{t}\right) = \sum_{i=1}^{n} \omega_n \boldsymbol{H}(\boldsymbol{S}_n). \tag{4}$$

The anisotropic anhysteretic algebraic model is derived from the measured major loops from 0° to 90° directly. Meanwhile, to evaluate the weights ω_{n} of the stop model, the minor loops of the sample M330-35 (2.4 Wt.% Si) are measured by RSST as well (Figure 8).

In this work seven stop operators are connected in parallel to model the anisotropic magnetic hysteresis properties of M330-35 (2.4 Wt.% Si). The weight of each stop operator ω_n is identified by fitting with measurements of Figure 8 using the least square algorithm. Comparisons between the measurements and the modelled data are shown in Figure 9 for

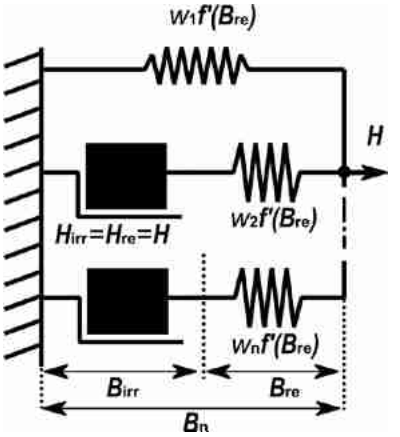

Figure 7.
Mechanical analogy of the vector stop hysteresis model

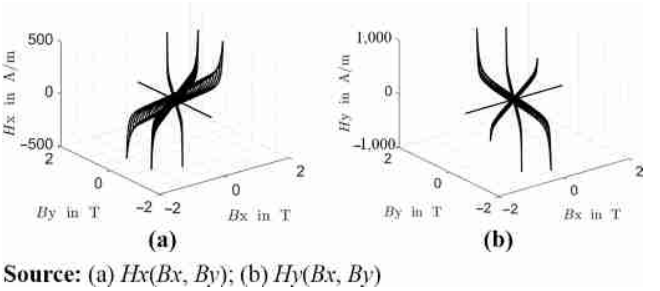

Source: (a) *Hx*(*Bx*, *By*); (b) *Hy*(*Bx*, *By*)

Figure 8.
Measured minor loops from 0.1 T to 1.6 T in steps of 0.1 T in the induction directions of 0°, 30°, 60° and 90°

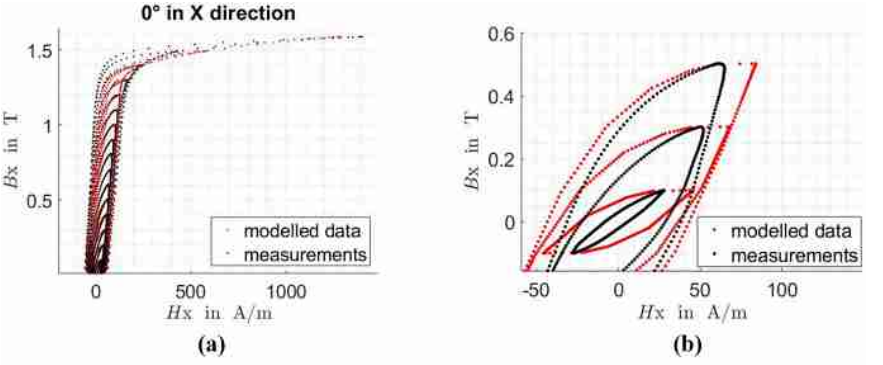

Source: (a) magnetic induction in 0°; (b) magnetic induction zoomed in 0.1T, 0.3T and 0.5T in 0°

Figure 9.
Comparison of the measured data under the magnetization amplitude from 0.1T to 1.6 T in a step of 0.1 T, with the simulated data obtained by the stop model with seven hysterons for electrical steel sheets M330-35 (2.4 Wt.% Si) in the induction direction 0°

induction direction 0° and in Figure 10 for induction direction 90°. A disagreement between the measured and the modelled hysteresis curves can be found especially on the minor loops and the knee (by induction from 1.2 T to 1.5 T) of the hysteresis loops. The reason for the especially obvious errors in the minor loops by small inductions such as 0.1 T to 0.4 T can be

that, the fitting with least square algorithm minimizes the errors preferentially on high magnetic inductions. To improve the accuracy in small induction ranges, the fitting algorithms should be adapted further for hysteresis characteristics with minor loops. The threshold of the stop model defines when the stop operator can be switched. Physically, it describes the magnitudes of the pinning fields, which are not constant as the magnetic field strength increased. It can be seen from the measurements, the hysteresis loop of the studied material M330-35 (2.4 Wt.% Si) is slimmer in the small induction range and larger in the knee range from 1.2 T to 1.5 T. However, the stop model presented in this work is constructed with constant threshold diagonal matrix. The error on the knee can be reduced by using more sophisticated modelled threshold surfaces instead of constant threshold values as presented in this study.

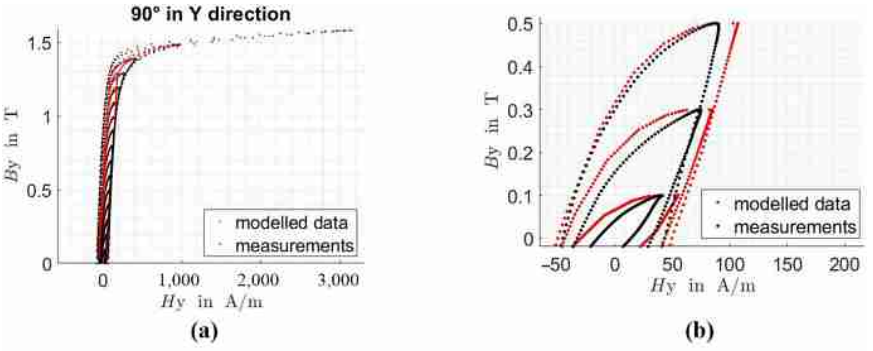

Source: (a) magnetic induction in 90°; (b) magnetic induction zoomed in 0.1T, 0.3T and 0.5T in 90°

Figure 10. Comparison of the measured data under the magnetization amplitude from 0.1T to 1.6 T in a step of 0.1 T, with the simulated data obtained by the stop model with seven hysterons for electrical steel sheets M330-35 (2.4 Wt.% Si)

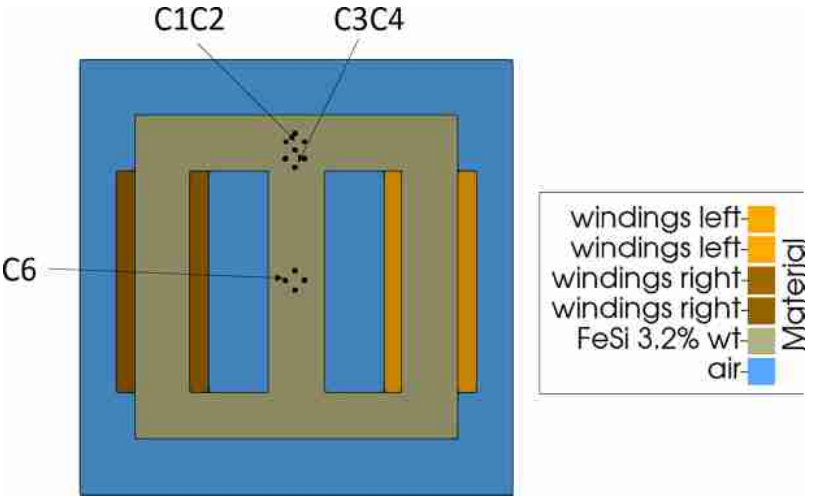

Figure 11. Qualitative description of the geometry of the model from TEAM workshop problem 32 (Bottauscio *et al.*, 2002) with pick-up coils for test case 2 and test case 3

4. Numerical study with TEAM workshop problem 32

The developed vector stop model is applied to the magnetic vector potential formulation of the FE solver to simulate the distribution of the flux density in electrical machines. In this paper, the TEAM workshop problem 32 is studied and the measurements are used to validate the vector stop hysteresis model. A qualitative description of the model is shown in Figure 11. The two dimensional model is a three limbs transformer with windings on the left and right limb (Bottauscio, *et al.*, 2002). The pick-up coils are placed in the core to measure the magnetic flux density. The most interesting cases are the test case 2 with harmonic magnetization and test case 3 with rotating magnetization. To simulate these two magnetization types, a vector hysteresis model is necessary.

As the vector hysteresis model describes the nonlinear anisotropic characteristics of the material, the Newton method is used as the interface between the material model and finite elements (FE) solver. The Newton method is a widely used iterative scheme to solve the nonlinear magnetic field problem with consideration of vector hysteresis. A schematic description of the incorporation of the material model into the FE simulation environment with Newton method is shown in Figure 12. Starting from the time step $t = 0$, the magnetic vector potential $A_{k=1}^{t=0}$ and magnetic flux density $\boldsymbol{B}_{k=1}^{t=0}$ are firstly initialized. With the input $\boldsymbol{B}_k^t$ and the memory state from the last time step $\boldsymbol{B}^{t-1}$ the vector stop hysteresis model provides for each time step and each Newton iteration step the 2×2 matrix of the partial derivatives $\boldsymbol{v}_\mathrm{d}$ and the magnetic field strength $\boldsymbol{H}_k^t$ for each element of the electrical steel sheet. The partial derivatives matrix $\boldsymbol{v}_\mathrm{d}$ is evaluated by means of numerical differentiation in the x and y directions, respectively. It should be positive definite to ensure a unique FE

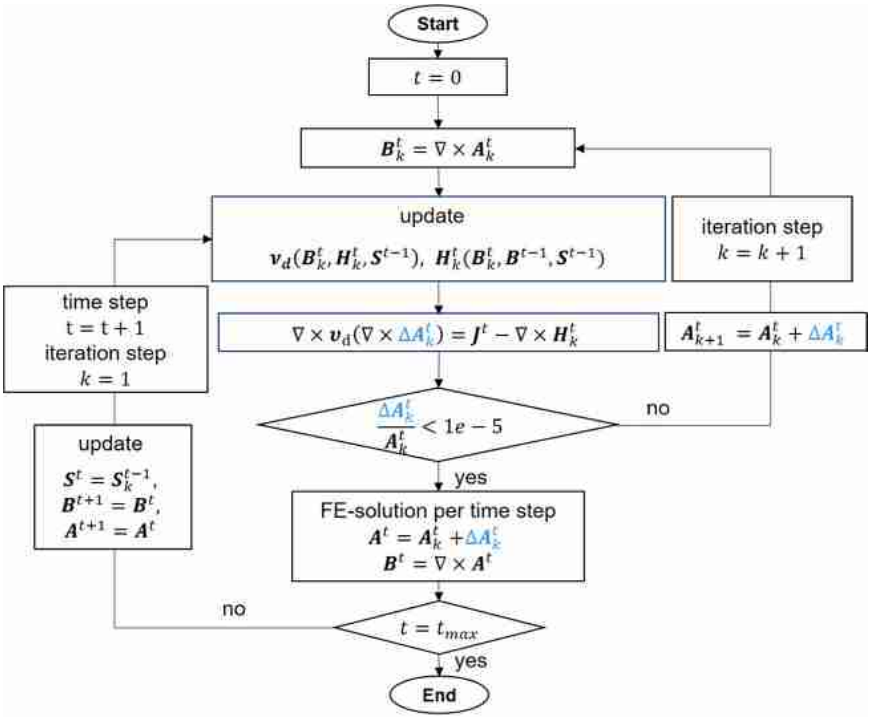

Figure 12.
Newton iteration scheme to solve the field problem with vector stop hysteresis model

solution and robust numerical calculation with Newton iteration. Solving the Newton formulation, the solution is determined when the relative increment of the magnetic vector potential is smaller than the defined tolerance. If the criterion is not satisfied, the magnetic vector potential will be updated and provided as the input for the next Newton iteration step. During the iteration the matrix $\boldsymbol{\nu}_{\mathrm{d}}$ and the vector $\boldsymbol{H}_k^l$ will be corrected until the solution fulfills Ampère's law with the excitation J^t of the time step t. During the Newton iteration, the memory of the vector stop hysteresis model is kept on the state from the last time step $\boldsymbol{B}^{t-1}$, which ensures a unique evolution of the hysteresis branches.

The validation of the vector stop hysteresis model and the numerical approach of the FE simulation is proceeded by comparing the simulated results with measurements. The results are depicted in Figure 13 for test case 2 with a harmonic magnetization and in Figure 14 for test case 3 with a rotating magnetization. The comparison shows an acceptable agreement.

By test case 2 when the current on the valley points, the biggest differences between measurements and simulated magnetic flux density can be observed. To minimize this error in minor loops the vector stop hysteresis model should be further investigated. The main reason can be that, for this test case seven stop operators are still not enough to represent the minor loops accurately. This results in the errors of fitting for weights. Another possibility for the lake of accuracy by representation the minor loops could be the choose of start point of Newton iterations, which have to be investigated and studied in future work. In this work the vector potential solution from the last time step is set as initial value for the Newton iteration of next time step, which could be not close enough to the solution corresponding to the current density at the valley points. To study this issue, the Newton formulation should be improved with an initialization technique. Furthermore, to identify whether the inaccuracy is derived from material model or iteration algorithm of FE simulation, the numerical calculation can also be implemented by fix point iteration methods with the same vector stop model (Dlala, 2011; Zhou, *et al.*, 2017).

By rotating magnetization the computated and measured B-Loci on C1C2 and C3C4 have similar routes and a satisfactory agreement.

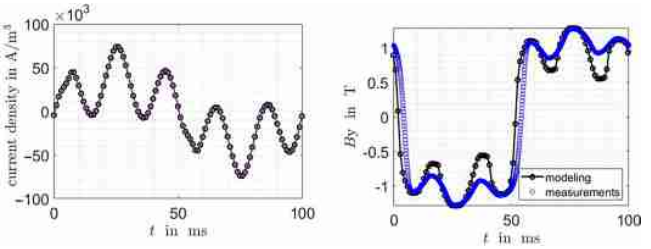

Figure 13.
Comparison of the simulated and the by the pick-up coil C6 measured magnetic flux density for test case 2

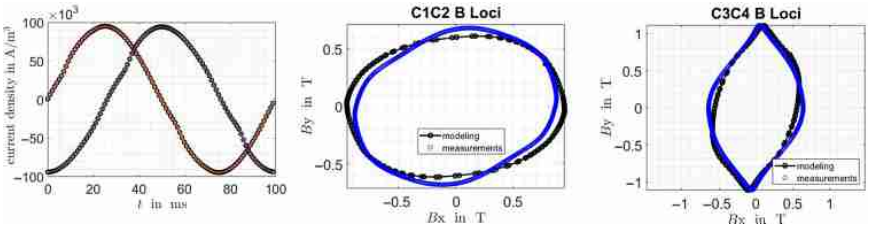

Figure 14.
Comparison of the simulated and by the pick-up coils C1C2 and C3C4 measured magnetic flux density for test case 3

5. Conclusions and further work

By integrating the anisotropic anhysteretic algebraic model into the elastic elements of the vector stop hysteresis model, the anisotropy in the permeability can appropriately be represented. Meanwhile, the model is able to represent the saturation properties and phase shifts between $\boldsymbol{H}$ and $\boldsymbol{B}$. The fitted parameters are based on the measured alternating hysteresis minor loops in four excitation directions. As the identified parameters are also valid for other magnetization types, such as harmonic and rotational excitations, no additional measurements are required. Comparison the modelled hysteresis loops with the measured data of M330-35 (2.4 Wt.% Si) obvious deviations can be observed in the small magnetic induction ranges. A proper fitting process to evaluate the weights of stop operators for hysteresis with minor loops should be further studied.

The FE simulation considering the hysteresis effects under harmonic and rotating magnetizations are presented. The vector stop hysteresis model and the numerical approach are validated with the measurements from TEAM workshop problem 32. Acceptable agreements between simulated and measured data can be stated. a satisfactory agreement, the implementation of the vector stop hysteresis model in the magnetic vector potential formulation with Newton method works properly. The vector stop hysteresis model can be further improved to simulate the realistic magnetic field in electrical machines. The aim of further studies is the development of an approach to evaluate the adapted number and distribution of stop hysterons to obtain a better agreement with measurements.

In this paper, the vector stop hysteresis model is constructed with constant threshold values. This means, no matter how large the excitation is for the material, the Barkhausen jumps will not vanish. Therefore, with constant threshold values the rotational hysteresis loss property cannot be represented correctly (Lin, *et al.*, 2014). Besides the influence on the rotational losses, a threshold surface which describes the properties of pinning fields can also minimize the deviations between measured and modelled data on knee ranges. A further work will be performed on the modeling of the threshold surfaces for plastic elements to prediction the hysteresis alternating and rotational losses correctly and improve the accuracy of representation the hysteresis loops with vector stop hysteresis model. The sample will be excited by rotating excitations, and the hysteresis stop model should be validated with the rotating measurements in terms of rotating hysteresis losses.

References

Bastos, J.P.A. and Sadowski, N. (2017), *Magnetic Materials and 3D Finite Element Modeling*, CRC press, Boca Raton.

Bastos, J.P.A., Hoffmann, K., Leite, J.V. and Sadowski, N. (2018), "A new and robust hysteresis modeling based on simple equations", *IEEE Transactions on Magnetics*, Vol. 54 No. 3, pp. 1-4. March.

Bavendiek, G., Leuning, N., Müller, F., Schauerte, B., Thul, A. and Hameyer, K. (2019), "Magnetic anisotropy under arbitrary excitation in finite element models", *Archives of Electrical Engineering*, Vol. 68 No. 2, pp. 455-466, April.

Bergqvist, A. (1997), "Magnetic vector hysteresis model with friction-like pinning", *Physica B: Condensed Matter*, Vol. 233 No. 4, pp. 342-347.

Bergqvist, A., Lundgren, A. and Engdahl, G. (1997), "Experimental testing of an anisotropic vector hysteresis model", *IEEE Transactions on Magnetics*, Vol. 33 No. 5, pp. 4152-4154, September.

Bottauscio, O., Chiampi, M., Ragusa, C., Rege, L. and Repetto, M. (2002), "A test case for validation of magnetic field analysis with vector hysteresis. Magnetics", *IEEE Transactions on Magnetics*, Vol. 38 No. 2, pp. 893-896.

Chwastek, K. (2013), "Anisotropic properties of non-oriented steel sheets", *IET Electric Power Applications*, Vol. 7 No. 7, pp. 573-579, August.

Dlala, E. (2011), "Efficient algorithms for the inclusion of the Preisach hysteresis model in nonlinear finite-element methods", *IEEE Transactions on Magnetics*, Vol. 47 No. 2, pp. 395-408, February.

Dlala, E., Saitz, J. and Arkkio, A. (2006), "Inverted and forward Preisach models for numerical analysis of electromagnetic field problems", *IEEE Transactions on Magnetics*, Vol. 42 No. 8, pp. 1963-1973, August.

Krasnosel'skii, M.A. and Pokrovskii, A.V. (1989), *Systems with Hysteresis*, Springer, Berlin Heidelberg.

Leite, J.V., Sadowski, N., Kuo-Peng, P., Batistela, N.J., Bastos, J.P.A. and De Espindola, A.A. (2004), "Inverse jiles–atherton vector hysteresis model", *IEEE Transactions on Magnetics*, Vol. 40 No. 4, pp. 1769-1775, July.

Leite, J.V., Sadowski, N., Kuo-Peng, P. and Bastos, J. (2005), "A new anisotropic vector hysteresis model based on stop hysterons", *IEEE Transactions on Magnetics*, Vol. 41 No. 5, pp. 1500-1503.

Leite, J.V., Sadowski, N., Da Silva, P.A., Batistela, N.J., Kuo-Peng, P. and Bastos, J.P. (2007), "Modeling magnetic vector hysteresis with play hysterons", *IEEE Transactions on Magnetics*, Vol. 43 No. 4, pp. 1401-1404.

Lin, D., Zhou, P. and Bergqvist, A. (2014), "Improved vector play model and parameter identification for magnetic hysteresis materials", *IEEE Transactions on Magnetics*, Vol. 50 No. 2, pp. 357-360, February.

Longhitano, M.R., Sixdenier, F., Scorretti, R., Geuzaine, C. and Krähenbühl, L. (2019), "Test-case transformer for the energy-based vector hysteresis model", *22nd International Conference on the Computation of Electromagnetic Fields (COMPUMAG)*.

Matsuo, T. and Shimasaki, M. (2001), "Isotropic vector hysteresis represented by superposition of stop hysteron models", *IEEE Transactions on Magnetics*, Vol. 37 No. 5, pp. 3357-3361.

Mayergoyz, I. (1991), *Mathematical Models of Hysteresis*, Springer, New York.

Pera, T., Ossart, F. and Waeckerle, T. (1993), "Field computation in non linear anisotropic sheets using the coenergy model", *IEEE Transactions on Magnetics*, Vol. 29 No. 6, pp. 2425-2427.

Shiozaki, M. and Kurosaki, Y. (1989), "Anisotropy of magnetic properties in non-oriented electrical steel sheets", *Textures and Microstructures*, Vol. 11 Nos 2/4, pp. 159-170, January.

Silvester, P.P. and Gupta, R.P. (1991), "Effective computational models for anisotropic soft BH curves", *IEEE Transactions on Magnetics*, Vol. 27 No. 5, pp. 3804-3807.

Steentjes, S., Henrotte, F. and Hameyer, K. (2016), "Energy-based ferromagnetic material model with magnetic anisotropy", *Journal of Magnetism and Magnetic Materials*, Vol. 425, pp. 20-24, October.

Visintin, A. (2006), "Chapter 1 - mathematical models of hysteresis", *The Science of Hysteresis*, Academic Press, Oxford, pp. 1-123.

Zhou, P., Lin, D., Lu, C., Rosu, M. and Ionel, D.M. (2017), "An adaptive fixed-point iteration algorithm for finite-element analysis with magnetic hysteresis", *IEEE Transactions on Magnetics*, Vol. 53 No. 10, pp. 1-5, October.

Corresponding author
Xiao Xiao can be contacted at: xiao.xiao@iem.rwth-aachen.de